NANO LETTERS

pubs.acs.org/NanoLett Letter

Crystal Size Effect on Carrier Transport of Microscale Perovskite Junctions via Soft Contact

Zhibin Zhao,[#] Wenduo Wang,[#] Xin Zhou, Lifa Ni, Keehoon Kang, Takhee Lee, Hong Han, Hongrui Yuan, Chenyang Guo, Maoning Wang, Min Jae Ko, Yuelong Li,* and Dong Xiang*

Cite This: *Nano Lett.* 2020, 20, 8640−8646 Read Online

ACCESS | Metrics & More | Article Recommendations | Supporting Information

ABSTRACT: To reduce the size of optoelectronic devices, it is essential to understand the crystal size effect on the carrier transport through microscale materials. Here, we show a soft contact method to probe the properties of irregularly shaped microscale perovskite crystals by employing a movable liquid metal electrode to form a self-adaptative deformable electrode−perovskite−electrode junction. Accordingly, we demonstrate that (1) the photocurrents of perovskite quantum dot films and microplatelets show profound differences regarding both the on/off ratio and the response time upon light illumination; and (2) small-size perovskite (<50 μm) junctions may show negative differential resistance (NDR) behavior, whereas the NDR phenomenon is absent in large-size perovskite junctions within the same bias regime. Our studies provide a method for studying arbitrary-shaped crystals without mechanical damage, assisting the understanding of the photogenerated carriers transport through microscale crystals.

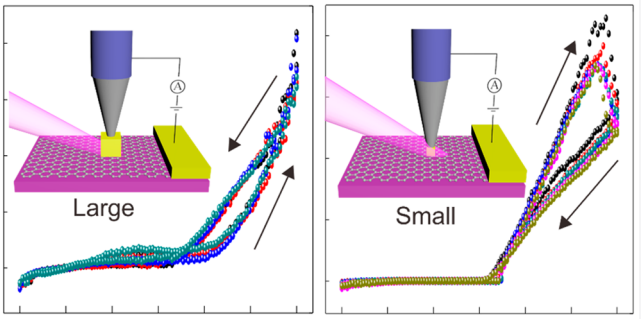

KEYWORDS: *perovskite single crystals, switches and rectifier, liquid metal electrode, negative differential resistance, size effect*

Hybrid organic−inorganic perovskites have attracted intensive attention in the past decade, among which organic lead trihalide $MAPbX_3$ (MA = CH_3NH_3, X = I, Br or Cl) is considered as a promising semiconductor due to its tunable bandgap,[1] high absorption coefficient,[2] low defect density,[3] long carrier lifetime, and diffusion length,[3,4] and these properties allow $MAPbX_3$ materials to be widely used in lasers,[5,6] light-emitting diodes,[7] solar cells,[8,9] sensors,[10,11] photodetectors,[12−14] and so forth. Although significant results using perovskite films have been reported, few studies have focused on smaller (μm or nm) perovskite single crystals although they may present distinctive properties compared to those of large perovskites (mm or cm). Apparently, typical methods (e.g., evaporating metal layers or spin coating conductive adhesives as electrodes) that are widely used for probing perovskite films are not suitable for microscale perovskites, especially when the perovskites are irregularly shaped. To address the properties of microscale perovskite crystals, (1) the size of the electrodes should be reduced to the microscale to match the size of the perovskite crystals, and the gap between the pair of electrodes should be precisely adjustable to fit the dimensions of the perovskite crystals; (2) it is better that the force between the perovskite and electrode can be adjusted to form a tight contact while avoiding damage (e.g., scratching and penetration); and (3) the contact is expected to be repeatable to allow repeated measurement for probing whether the carrier transport features are reproducible.

To this end, we developed a soft contact method by employing liquid EGaIn (eutectic of gallium and indium) as the top electrodes and a flat Ag^{TS} (template-stripped Ag substrates) or graphene layer as the bottom electrode. This soft contact strategy was applied to construct stable perovskite junctions, that is, to sandwich $CH_3NH_3PbBr_3$ ($MAPbBr_3$) crystals with top and bottom electrodes. The adaptive deformation of the EGaIn electrode makes it feasible to create a stable and tight electrode−perovskite contact without significant mechanical damage to the samples. Subsequently, the optoelectrical properties of both $MAPbBr_3$ microplatelet (MP) and $MAPbBr_3$ quantum dot (QD) films were investigated. Compared to those of small quantum dot (≤10 nm) films, the perovskite microplatelets showed a faster photocurrent response with a much higher on/off switch ratio upon light illumination.

Received: August 17, 2020
Revised: November 19, 2020
Published: November 25, 2020

https://dx.doi.org/10.1021/acs.nanolett.0c03347
Nano Lett. 2020, 20, 8640−8646

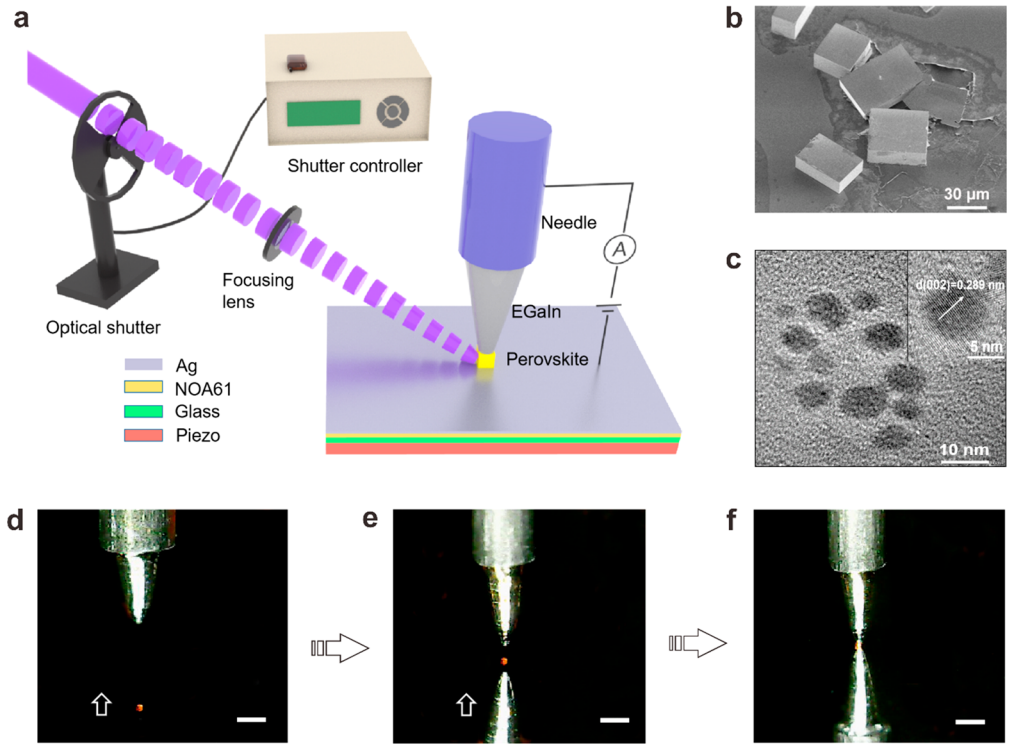

Figure 1. Diagram of the optoelectrical measurement system and images of the perovskite crystals and quantum dots. (a) Via the modulation of a chopper, the pulsed laser irradiates a perovskite microplatelet (or quantum dot film). The perovskite crystal is sandwiched between a top EGaIn tip and a bottom Ag^{TS} substrate which is composed of a silver film, a Norland optical adhesive (NOA61) layer, and a glass substrate. (b) SEM image of cubic-shaped $MAPbBr_3$ microplatelets. (c) HR-TEM image of $MAPbBr_3$ quantum dots. Inset: magnified area of the HR-TEM image. (d–f) The formation of EGaIn–perovskite–Ag^{TS} junctions with irregularly shaped perovskites by the upward movement of the substrate via piezo control. A mirror image of the top EGaIn tip is observed on the surface of the bottom Ag^{TS} substrate. The arrows indicate the movement direction of the bottom Ag^{TS} substrate. Scale bar: 200 μm.

Negative differential resistance (NDR), characterized by a decrease in current with increasing voltage, has attracted tremendous attention and has been regarded as an important element for nanoelectronic applications in low power memory, high frequency oscillators, and logic circuit applications.[15−18] Typically, NDR can be achieved via resonant tunnelling heterostructures with a system composed of double potential barriers and one potential well.[19,20] NDR behavior has also been observed in sandwiched membranes, which was normally attributed to charge-carrier trapping/detrapping by defects.[21,22] Here, we observed an intrinsic and pronounced room-temperature NDR effect with relatively small-size (~30 μm) perovskite MP junctions, whereas the NDR behavior disappeared for large (~80 μm) perovskite MP junctions, indicating a mechanism different from that in the previous literature. A model based on ion migration and enhanced carrier recombination in perovskites was developed to illustrate the size-dependent NDR behavior of the perovskites.

RESULTS AND DISCUSSION

We use an ultraflat Ag^{TS} substrateor graphene layer as the moveable bottom electrode (Supplementary Figures S1−S3)[23] and use EGaIn as the fixed top electrode (Figure S4).[24,25] Figure 1a shows the experimental setup. Via the modulation of a chopper, the perovskite MP or QD film is periodically irradiated by a laser with a wavelength of 405 nm. Controlled by a piezo actuator, the bottom Ag^{TS} substrate can be moved up or down with subnanometer precision. In this way, the perovskite MP or perovskite QD film can be precisely sandwiched between the EGaIn tip and Ag^{TS} substrate. Figure 1b presents a scanning electron microscope (SEM) image of the $MAPbBr_3$ MPs under investigation. The MPs have clear edges and square corners, indicating the high quality of the MPs.[26,27] Figure 1c shows high-resolution transmission electron microscopy (HR-TEM) images of the $MAPbBr_3$ QDs. The $MAPbBr_3$ lattice index is the plane (002), and the calculated *d*-space is approximately 0.3 nm.[28,29] The size of the QDs falls in the regime between 3.0 and 8.0 nm.

Figure 1d–f displays a series of photos captured by a digital electron microscope during the formation process of the EGaIn–MP–Ag^{TS} junctions via the upward movement of the Ag^{TS} substrate. To ensure that the needle tip directly contacts the perovskite MP, two digital microscopes set in orthogonal directions with different view angles were used to monitor the contact process (Figure S5). A close examination of the tip image shows that adaptive deformation of the liquid metal electrode occurs to match the surface topography of the perovskite MPs. For example, a small amount of pressure between the EGaIn electrode and ball-shaped perovskite results in a denting of the EGaIn at the contact point (Figure S6 and Video S1). In this way, a stable and tight contact can be constructed, which facilitates the following optoelectrical measurements. This physical soft contact does not cause contamination or mechanical damage[30] and can be repeatedly performed hundreds of times.

Under a fixed bias voltage (0.5 V), the real-time current response of the EGaIn–MP–Ag^{TS} junction (denoted the MP junction) under laser illumination (λ = 405 nm, chopper ratio

https://dx.doi.org/10.1021/acs.nanolett.0c03347
Nano Lett. 2020, 20, 8640−8646

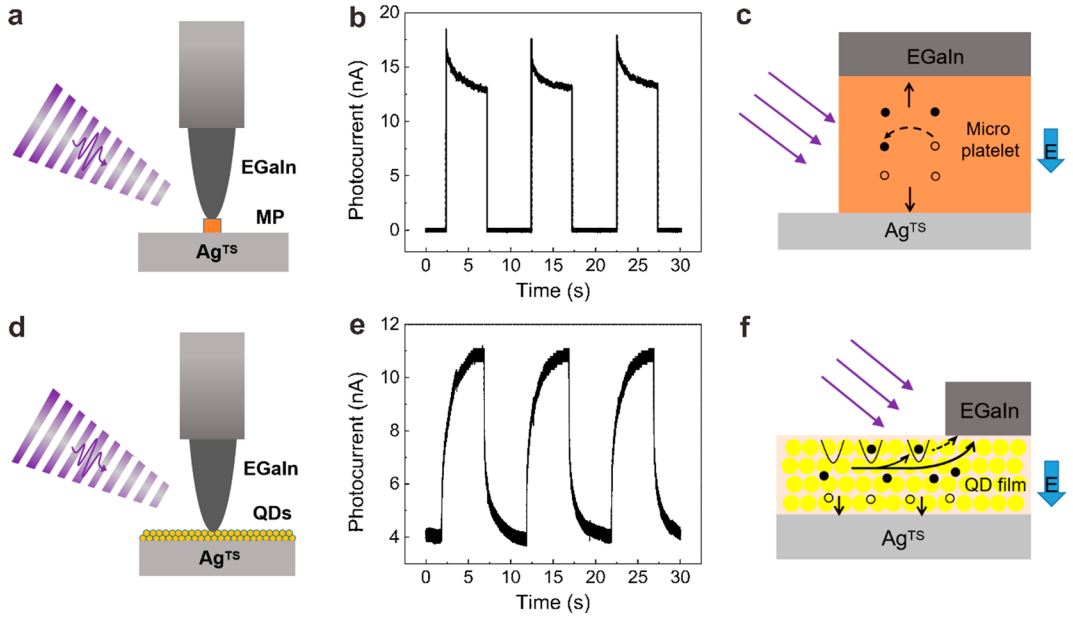

Figure 2. Schematics of two types of junctions and the corresponding photodynamic responses. (a) The structure diagram of the EGaIn−MP−Ag^{TS} junction. (b) A spike in the photocurrent was observed under light illumination for MP junction. (c) The mechanism for the spike observation presented in part b. A large number of photogenerated carriers leads to a fast increase in the current under light illumination. The recombination of the carriers leads to a decay in the current. (d) The structure diagram of the EGaIn−QDs−Ag^{TS} junction. (e) The photocurrent increases slowly under light illumination and decreases slowly when the light is turned off for QD film junctions. (f) Trapping events by defects result in a slow increase in the current under light illumination, and detrapping events lead to a slow decrease in the current when the light is turned off.

0.1 Hz) is recorded, as shown in Figure 2a,b. The current increases quickly followed by a decay to a steady state under light illumination, that is, a spike in the photocurrent is observed. This spike becomes more obvious when the light intensity or the bias voltage is increased, see Figure S7. The photocurrent drops sharply to a very low value (close to zero) when the light is turned off. Compared to the MP junctions, the QD film junctions as presented in Figure 2d,e, show significant differences: (1) under light illumination, the spike observed for the MP junctions is absent and is replaced by a slowly continuous growth; (2) the current drops rapidly in the MP junctions when the light is turned off, but the current decays slowly for the QD junctions; and (3) the dark current in the QD junctions is much higher than that in the MP junctions, resulting in a very large variation in the on/off ratios, that is, $R_{on/off} \approx 500$ for MP junctions and $R_{on/off} \approx 3$ for QD film junctions.

The underlying mechanisms for the significant differences between the two types of junctions are discussed as follows. The QD film has more defects than the MPs due to that (1) a single QD has a higher surface to volume ratio than a MP, thus possessing a higher density of defects which are generally located at the surface of the perovskite;[31] (2) there are substantial grain boundaries within the QD film, which serve as additional trapping centers; (3) the large area of the QD film illuminated by light and the correspondingly long diffusion distance (i.e., the carriers far away from the needle tip move toward the tip electrodes also) result in a high probability for the carriers to be trapped by the defects, as shown in Figure 2f. Accordingly, the photocurrent response of the QD film junction will be strongly affected by the carrier trapping and detrapping events in which the trapping events suppress a fast increase of the photocurrent upon light illumination, while the detrapping process hinders the fast reduction of the current when the light is turned off, as observed in Figure 2e. In contrast, the perovskite MPs have fewer defects and thus negligible issues of trapping and detrapping. Therefore, the dynamic response of the photocurrent in the MP junction is mainly dominated by the carrier generation and recombination process, rather than trapping and detrapping processes. Under light illumination, a large number of photogenerated carriers in MP lead to a fast increase in the current, followed by a decay in the current due to carrier recombination,[32] which results in a spike feature in the current curve, as shown in Figure 2c.

To fully understand the properties of carrier transport, $I-V$ measurements were performed, which show strong rectification behavior, see Figure S8. More interestingly, we find that the $I-V$ characteristics are strongly dependent on the size of the perovskite crystals when the bottom Ag^{TS} electrodes are replaced by graphene electrodes (Figure 3). A hysteresis feature is clearly observed in the positive bias regime for a large-size perovskite (~80 μm in length, treated as a cube), see Figure 3a. In contrast, NDR is observed for small-size perovskites (~30 μm), as presented in Figure 3c. To the best of our knowledge, the NDR behavior of the photocurrent dependent on the perovskite crystal size has not been reported so far.

Here, we focus on the size-dependent NDR behavior and try to reveal the underlying mechanism. We know that the large crystals are distinguished from small crystals in two aspects: (1) The smaller perovskite crystals possess a higher surface-to-volume ratio. Although the perovskite single crystals prepared by our method are quite stable, showing no significant chemical decomposition over several weeks,[33] the perovskites may unavoidably absorb some water during storage and measurement processes.[34] The small-size perovskite may adsorb enough water, which may permeate through the whole perovskite and thus facilitates the migration of ions

https://dx.doi.org/10.1021/acs.nanolett.0c03347
Nano Lett. 2020, 20, 8640−8646

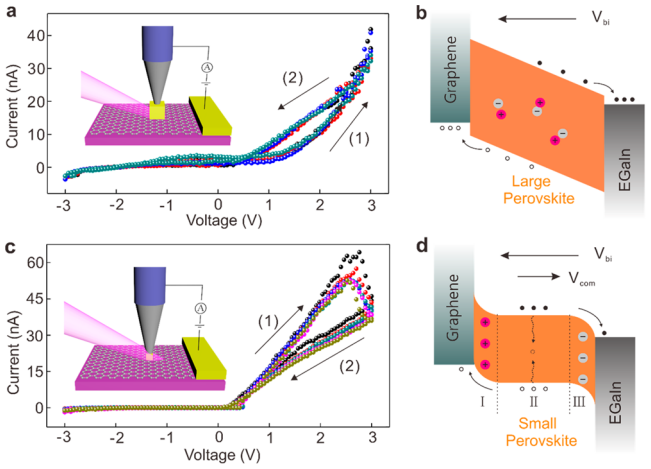

Figure 3. *I*–*V* curves and the mechanism for the NDR observations. (a) The measured *I*–*V* curves for large perovskite under light illumination. (1) and (2) indicate forward sweep and backward sweep. Inset: Schematic of the EGaIn–perovskite–graphene junction. (b) Band alignment of large-size perovskite junction when a positive voltage (V_{bi}) is applied to the EGaIn electrode. A uniform potential drop in V_{bi} appears inside the perovskite layer. (c) The *I*–*V* curves for small-size perovskite upon light illumination. NDR behavior is observed under a positive bias. (d) Band alignment of small-size perovskite junction changes induced by ionic migration. Under a strong external field, the ionic separation and accumulation at the electrode/perovskite interface results in a compensating field (V_{com}) which in turn screens the external applied field.

under an applied electric field. (2) The smaller perovskite crystals experience higher electrical fields under the same bias voltage. Here, we believe that the effect of field strength should be the main reason for NDR observation based on the facts that NDR only appears with small size perovskite.

The migration of $CH_3NH_3^+$ and halide ions under an electric field in hybrid organic–inorganic perovskites has been previously reported and analyzed.[35−38] In our case, the electric field in large perovskites is weaker than that of small perovskites at the same bias voltage. Accordingly, the migration of ions does not occur due to an insufficient electric field for initiating ion migration in the large perovskite. In this case, a uniform potential drop of V_{bi} may appear inside the perovskite layer (the Schottky barrier at the interface is not shown for simplicity), which facilitates the separation of photogenerated carriers and promotes the extraction of free carriers, as shown in Figure 3b. In contrast, for small perovskites, cations and anions may move to the graphene and EGaIn driven by the strong applied field (V_{bi}). Accordingly, the accumulation of ions at the interface will result in a compensating field (V_{com}) opposite the externally applied field. When the compensating field increases to a value equal to that of the external field, the externally applied field is totally screened.[37] Correspondingly, the energy band in region II becomes flat, and the potential drop in V_{bi} occurs only in regions I and III, as shown in Figure 3d. The accumulation of the ions at the interface leads to the following events: (1) the diffusion of carriers to the electrodes is hindered, and the extraction efficiency of free carriers in region II is reduced due to the effect of V_{com}; and (2) due to the flat energy band in region II, carriers cannot be separated efficiently so that the recombination of holes and electrons is enhanced. These factors induced by ion acumination suppress the current and thus result in NDR behavior.

According to pioneering studies, the NDR behavior is normally related to charge trapping/detrapping events due to defects.[34,39−41] Here, we argue that the NDR behavior in our observation does not mainly originate from the trapping/detrapping events due to the following: (1) The dynamic measurement of the photocurrent as a function of time shows that the photocurrent sharply decreases to zero when the light is turned off (Figure S7). This observation indicates that there are few defects in our perovskite single crystals and that trapping/detrapping does not dominate the carrier transport because the detrapping of carriers will lead to a slow decay in photocurrent when the light is turned off. (2) The carrier trapping/detrapping at the interface strongly depends on the sweep direction of the applied voltage.[40] Carrier trapping/detrapping-induced NDR disappears if voltage sweeping is performed only in one sign of bias regime (i.e., a voltage sweep only in the positive bias regime or only in the negative bias regime).[34,40] However, clear NDR behavior is observed in our experiments when the voltage sweep is performed solely in the positive bias regime, as shown in Figure S9. (3) NDR behavior is not observed in the EGaIn–perovskite–Ag^{TS} junction (regardless of the crystal size, Figure S9) which will be addressed later.

The dynamic measurement of photocurrent as a function of time for both small and large perovskites is presented in Figure 4. As a common feature, the photocurrent decreases sharply to

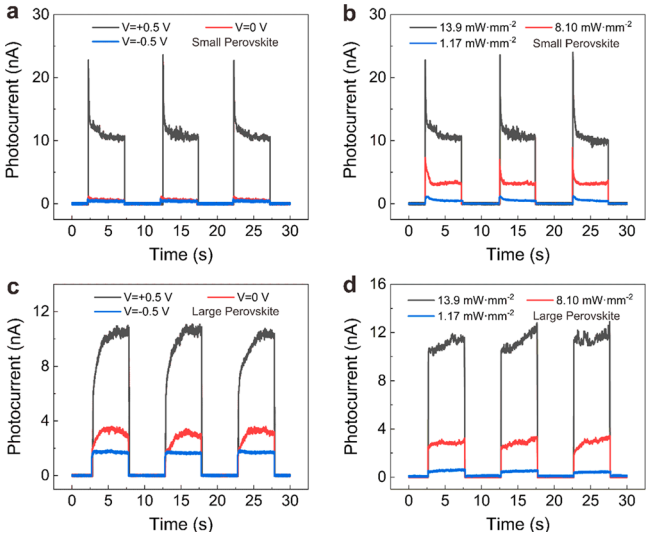

Figure 4. Photocurrent responses under light illumination for small and large perovskites. (a,c) The real-time photocurrent of the EGaIn–perovskite–graphene junctions with (a) small size perovskite and (c) large size perovskite under different bias voltages (light intensity ~13.9 mW·mm^{-2}). The zero-bias photocurrent in large-size perovskite junctions is much higher than that in small-size perovskite junctions. (b,d) The real-time photocurrent responses of the junction with (b) small size perovskite and (d) large size perovskite under different light intensities (V_{bi} = 0.5 V).

zero when the light is turned off, which indicates that there are few trapping/detrapping events in both small and large perovskites. There are two distinct features for small (~30 μm) and large-size perovskite (~80 μm). First, for small-size perovskite junctions the photocurrent spikes degenerate as the bias voltage or light intensity decreases (Figure 4a,b). In contrast, the spike disappears for large perovskites (Figure 4c,d) regardless of the bias voltage and light intensity. We

https://dx.doi.org/10.1021/acs.nanolett.0c03347
Nano Lett. 2020, 20, 8640−8646

attribute the spike presented by the small perovskite junction to the highly efficient separation of carriers by the strong applied electrical field, which results in a fast increase in the current in the small-size perovskite. Second, the small size perovskite shows a very low photocurrent at zero bias voltage (Figure 4a). In contrast, the large size perovskite shows a much higher photocurrent at zero bias voltage despite the long diffusion distance for carriers to reach the electrodes (Figure 4c). We attribute this difference to the fact that photogenerated carriers are much more abundant in large perovskites than in small perovskites. Because of the effect of the built-in electric field at the asymmetric junction, photogenerated carriers can be extracted by the electrodes at zero bias voltage.[42] Thus, a high photocurrent is reasonable for a large perovskite junction.

The open question is that NDR behavior is not observed in the EGaIn−MP−Ag^{TS} junction when the graphene electrode is replaced by Ag^{TS} electrode, regardless of the size of perovskite crystals, as shown in Figure S9. The EGaIn−MP−graphene junction has similar energy landscape within the junction as EGaIn−MP−Ag^{TS}. Therefore, the observed NDR behavior may be related to the specific surface area of the electrode material and the electrode material's affinity toward the ion species. Carbon-based materials are likely to adsorb ions on their surface via van der Waals force or surface functional groups,[43] thus it is easier for the ions to be accumulated stably on the graphene/perovskite interface. It was reported that the charged ions in the perovskite crystal drifted and accumulated in the interface between carbon-based electrode (e.g., carbon nanotube and graphene) and perovskite under the applied electric field.[44,45] For Ag^{TS} electrode, the halide ions may electrochemically react with Ag^{TS} electrode (e.g., $Br^- + Ag^+ >$ AgBr, see Supporting Information Figure S11); this redox reaction (unlike physical adsorption) will reduce the number of ions at the interface instead of accumulating ions. Therefore, the absence of NDR behavior in EGaIn−perovskite−Ag^{TS} junction might due to the poor possibility of ion accumulation on the Ag/perovskite interface. Finally, we want to point out that we had probed the properties of the perovskite QD films and perovskite microplatelets with dimensions varied from dozens of micrometers to hundreds of micrometers. However, it is still a challenge to probe a single perovskite crystal with dimension comparable to wavelength due to the short circuit problem induced by the deformation of the electrode. To solve this problem, making a sharper tip and improving the hardness of the liquid metal electrode is highly expected. Alternatively, using conductive atomic force microscope (CAFM) can be a good choice to avoid short problem.

CONCLUSIONS

A soft contact method for sandwiching microscale perovskite crystals was developed, providing a platform for studying microscale materials with various sizes. We demonstrate, for the first time, that size-effect plays a critical role in determining the properties of carrier transport through perovskite junctions, as far as the size of the crystals is reduced to microscale regime. It is revealed that the photocurrent in perovskite MPs is mainly influenced by carrier generation and recombination events, whereas the photocurrent in perovskite QD films is mainly affected by trapping/detrapping events. Moreover, a size-dependent NDR is observed that is unrelated to charge trapping. The underlying mechanisms are further clarified in that the size-dependent NDR should originate from ion migration upon strong field and correspondingly enhanced carrier recombination in small size perovskites. The microlevel measurements pave a way for better scrutinizing the heterogeneous properties of nanoscale or microscale perovskites, assisting to reduce the size of photoelectronic devices employing perovskite crystals.

EXPERIMENTAL SECTION

Characterization of Ag^{TS} and Perovskite Crystal. The roughness of the Ag^{TS} surface was determined by Innova AFM using trapping-mode tips with intermittent contact (resonant frequency f_0 = 525 kHz, force constant k = 200 N/m) and analyzed using the NanoScope Analysis 1.8 software package. XRD patterns were measured by X-ray diffraction (Rigaku ATX-XRD) with Cu Kα radiation (k = 1.5405 Å) at 10° min^{-1}. PL measurement was performed by a spectrometer (Edinburgh FS5) at room temperature with a laser wavelength of 380 nm. The morphology of the perovskite microplatelet was characterized by field-emission SEM (JEOL JSM-7800F). The high-resolution TEM image was obtained by transmission electron microscopy (TEM, JEOL JEM-2000EX) with fast operation at 200 kV. The detailed data regarding AFM, XRD, and PL can be found in Figure S10.

Photocurrent Measurements. The position and movement of the bottom Ag^{TS} electrode are controlled by PiezoWalk actuators (PI, N-111, Germany), which can move continuously in the vertical direction with a resolution of 0.1 nm and a maximum travel range of 10 mm. A semiconductor laser (MW-ZL-405/1−200 mW) with a wavelength of 405 nm laser was used as the light illumination source, and the light power was measured by a light power meter (Thorlabs PM400D). The Daheng Optics' GCI-73 M (resolution 1 ms) electronic timer and series shutters were used to control the period of light illumination. The real-time current response upon light irradiation is recorded in ambient with relative humidity of ∼30% by a semiconductor analyzer (B1500A, KEYSIGHT).

ASSOCIATED CONTENT

Supporting Information

The Supporting Information is available free of charge at https://pubs.acs.org/doi/10.1021/acs.nanolett.0c03347.

Device fabrication and characterization, material synthesis and characterization, photocurrent response and explanation of rectification mechanism of EGaIn-perovskite-Ag^{TS} junctions, and additional experiments about EGaIn-perovskite-graphene junctions (PDF)

Video S1, adaptive deformation of EGaIn electrode (MP4)

Video S2, hysteresis behavior is observed for large-size perovskite during the $I-V$ measurement (MP4)

Video S3, NDR behavior is observed for small-size perovskite during the $I-V$ measurement (MP4)

AUTHOR INFORMATION

Corresponding Authors

Yuelong Li − *Institute of Photoelectronic Thin Film Devices and Technology, Key Laboratory of Photoelectronic Thin Film Devices and Technology of Tianjin, Solar Energy Research Center, Nankai University, Tianjin 300350, China;* orcid.org/0000-0003-0168-6107; Phone: 0086-137-5223-8217; Email: lyl@nankai.edu.cn

https://dx.doi.org/10.1021/acs.nanolett.0c03347
Nano Lett. 2020, 20, 8640−8646

Dong Xiang − *Tianjin Key Laboratory of Micro-scale Optical Information Science and Technology, Institute of Modern Optics and Center of Single Molecule Sciences, College of Electronic Information and Optical Engineering, Nankai University, Tianjin 300350, China;* orcid.org/0000-0002-5632-6355; Phone: 0086-151-022-44129; Email: xiangdongde@nankai.edu.cn

Authors

Zhibin Zhao − *Tianjin Key Laboratory of Micro-scale Optical Information Science and Technology, Institute of Modern Optics and Center of Single Molecule Sciences, College of Electronic Information and Optical Engineering, Nankai University, Tianjin 300350, China*

Wenduo Wang − *Institute of Photoelectronic Thin Film Devices and Technology, Key Laboratory of Photoelectronic Thin Film Devices and Technology of Tianjin, Solar Energy Research Center, Nankai University, Tianjin 300350, China*

Xin Zhou − *Institute of Photoelectronic Thin Film Devices and Technology, Key Laboratory of Photoelectronic Thin Film Devices and Technology of Tianjin, Solar Energy Research Center, Nankai University, Tianjin 300350, China*

Lifa Ni − *Tianjin Key Laboratory of Micro-scale Optical Information Science and Technology, Institute of Modern Optics and Center of Single Molecule Sciences, College of Electronic Information and Optical Engineering, Nankai University, Tianjin 300350, China*

Keehoon Kang − *Department of Physics and Astronomy, and Institute of Applied Physics, Seoul National University, Seoul 08826, Korea;* orcid.org/0000-0003-1230-3626

Takhee Lee − *Department of Physics and Astronomy, and Institute of Applied Physics, Seoul National University, Seoul 08826, Korea;* orcid.org/0000-0001-5988-5219

Hong Han − *Institute of Photoelectronic Thin Film Devices and Technology, Key Laboratory of Photoelectronic Thin Film Devices and Technology of Tianjin, Solar Energy Research Center, Nankai University, Tianjin 300350, China*

Hongrui Yuan − *Tianjin Key Laboratory of Micro-scale Optical Information Science and Technology, Institute of Modern Optics, Nankai University, Tianjin 300350, China*

Chenyang Guo − *Tianjin Key Laboratory of Micro-scale Optical Information Science and Technology, Institute of Modern Optics and Center of Single Molecule Sciences, College of Electronic Information and Optical Engineering, Nankai University, Tianjin 300350, China*

Maoning Wang − *Tianjin Key Laboratory of Micro-scale Optical Information Science and Technology, Institute of Modern Optics and Center of Single Molecule Sciences, College of Electronic Information and Optical Engineering, Nankai University, Tianjin 300350, China*

Min Jae Ko − *Department of Chemical Engineering, Hanyang University, Seoul 04763, Korea;* orcid.org/0000-0002-4842-3235

Complete contact information is available at: https://pubs.acs.org/10.1021/acs.nanolett.0c03347

Author Contributions

#Z.Z. and W.W. contributed equally.

Author Contributions

The manuscript was written through contributions of all authors. All authors have given approval to the final version of the manuscript.

Notes

The authors declare no competing financial interest.

■ ACKNOWLEDGMENTS

We thank Prof. Jingshan Luo, Prof. Weihua Wang, and Prof. Weichao Wang for fruitful discussion. We acknowledge the financial support from the National Natural Science Foundation of China (91950116, 61571242, 11804170, 61775105, 61874167, 11504270), National Key R&D Program of China (Grant 2018YFB1500105), National Creative Research Laboratory program (Grant 2012026372) through the National Research Foundation of Korea, Natural Science Foundation of Tianjin City (19JCZDJC31000, 19JCJQJC60900, 17JCYBJC41400), and the 111 Project (B16027), the International Cooperation Base (2016D01025).

■ REFERENCES

(1) Jeng, J. Y.; Chiang, Y. F.; Lee, M. H.; Peng, S. R.; Guo, T. F.; Chen, P.; Wen, T. C. $CH_3NH_3PbI_3$ perovskite/fullerene planar-heterojunction hybrid solar cells. *Adv. Mater.* **2013**, *25*, 3727−3732.

(2) Burschka, J.; Pellet, N.; Moon, S. J.; Humphry-Baker, R.; Gao, P.; Nazeeruddin, M. K.; Gratzel, M. Sequential deposition as a route to high-performance perovskite-sensitized solar cells. *Nature* **2013**, *499*, 316−319.

(3) Wei, H.; et al. Sensitive X-ray detectors made of methylammonium lead tribromide perovskite single crystals. *Nat. Photonics* **2016**, *10*, 333−339.

(4) Bi, Y.; Hutter, E. M.; Fang, Y.; Dong, Q.; Huang, J.; Savenije, T. J. Charge carrier lifetimes exceeding 15 μs in methylammonium lead iodide single crystals. *J. Phys. Chem. Lett.* **2016**, *7*, 923−928.

(5) Xing, G.; Mathews, N.; Lim, S. S.; Yantara, N.; Liu, X.; Sabba, D.; Gratzel, M.; Mhaisalkar, S.; Sum, T. C. Low-temperature solution-processed wavelength-tunable perovskites for lasing. *Nat. Mater.* **2014**, *13*, 476−480.

(6) Ha, S.-T.; Shen, C.; Zhang, J.; Xiong, Q. Laser cooling of organic-inorganic lead halide perovskites. *Nat. Photonics* **2016**, *10*, 115−121.

(7) Seo, H.-K.; et al. Efficient flexible organic/inorganic hybrid perovskite light-emitting diodes based on graphene anode. *Adv. Mater.* **2017**, *29*, 1605587.

(8) Mei, A.; et al. A hole-conductor-free, fully printable mesoscopic perovskite solar cell with high stability. *Science* **2014**, *345*, 295−298.

(9) Liu, M.; Johnston, M. B.; Snaith, H. J. Efficient planar heterojunction perovskite solar cells by vapour deposition. *Nature* **2013**, *501*, 395−398.

(10) Yakunin, S.; Dirin, D. N.; Shynkarenko, Y.; Morad, V.; Cherniukh, I.; Nazarenko, O.; Kreil, D.; Nauser, T.; Kovalenko, M. V. Detection of gamma photons using solution-grown single crystals of hybrid lead halide perovskites. *Nat. Photonics* **2016**, *10*, 585−589.

(11) Wei, H.; Huang, J. Halide lead perovskites for ionizing radiation detection. *Nat. Commun.* **2019**, *10*, 1066.

(12) Wu, T.; Ahmadi, M.; Hu, B. Giant current amplification induced by ion migration in perovskite single crystal photodetectors. *J. Mater. Chem. C* **2018**, *6*, 8042−8050.

(13) Murali, B.; Saidaminov, M. I.; Abdelhady, A. L.; Peng, W.; Liu, J.; Pan, J.; Bakr, O. M.; Mohammed, O. F. Robust and air-stable sandwiched organo-lead halide perovskites for photodetector applications. *J. Mater. Chem. C* **2016**, *4*, 2545−2552.

(14) Ahmadi, M.; Wu, T.; Hu, B. A review on organic-inorganic halide perovskite photodetectors: Device engineering and fundamental physics. *Adv. Mater.* **2017**, *29*, 1605242.

(15) Kim, K.-H.; et al. A multiple negative differential resistance heterojunction device and its circuit application to ternary static random access memory. *Nanoscale Horiz.* **2020**, *5*, 654−662.

(16) Kadhim, M. S.; Yang, F.; Sun, B.; Wang, Y.; Guo, T.; Jia, Y.; Yuan, L.; Yu, Y.; Zhao, Y. A resistive switching memory device with a

negative differential resistance at room temperature. *Appl. Phys. Lett.* **2018**, *113*, 053502.
(17) Sattari-Esfahlan, S. M. Multi-peak negative differential resistance in silicene superlattice: Toward multi-valued silicene logic devices. *J. Appl. Phys.* **2018**, *123*, 244503.
(18) Suzuki, S.; Asada, M.; Teranishi, A.; Sugiyama, H.; Yokoyama, H. Fundamental oscillation of resonant tunneling diodes above 1 THz at room temperature. *Appl. Phys. Lett.* **2010**, *97*, 242102.
(19) Du, R.; Qiu, X.; Li, A.; Wu, D. Ferroelectric modulation on resonant tunneling through perovskite double-barriers. *Appl. Phys. Lett.* **2014**, *104*, 142907.
(20) Agrawal, K.; Gupta, V.; Srivastava, R.; Rajput, S. S. Perovskite resonant tunneling FET with sequential negative differential resistance peaks. *ACS Appl. Electron. Mater.* **2019**, *1*, 735−744.
(21) Jia, C. H.; Sun, X. W.; Li, G. Q.; Chen, Y. H.; Zhang, W. F. Origin of attendant phenomena of bipolar resistive switching and negative differential resistance in $SrTiO_3$:Nb/ZnO heterojunctions. *Appl. Phys. Lett.* **2014**, 104.
(22) Yang, G.; Jia, C. H.; Chen, Y. H.; Chen, X.; Zhang, W. F. Negative differential resistance and resistance switching behaviors in $BaTiO_3$ thin films. *J. Appl. Phys.* **2014**, *115*, 204515.
(23) Simeone, F. C.; Yoon, H. J.; Thuo, M. M.; Barber, J. R.; Smith, B.; Whitesides, G. M. Defining the value of injection current and effective electrical contact area for EGaln-based molecular tunneling junctions. *J. Am. Chem. Soc.* **2013**, *135*, 18131−18144.
(24) Dickey, M. D.; Chiechi, R. C.; Larsen, R. J.; Weiss, E. A.; Weitz, D. A.; Whitesides, G. M. Eutectic Gallium-Indium (EGaIn): A liquid metal alloy for the formation of stable structures in microchannels at room temperature. *Adv. Funct. Mater.* **2008**, *18*, 1097−1104.
(25) Fracasso, D.; Valkenier, H.; Hummelen, J. C.; Solomon, G. C.; Chiechi, R. C. Evidence for quantum interference in SAMs of arylethynylene thiolates in tunneling junctions with eutectic Ga-In (EGaIn) top-contacts. *J. Am. Chem. Soc.* **2011**, *133*, 9556−9563.
(26) Galisteo-Lopez, J. F.; Li, Y.; Miguez, H. Three-dimensional optical tomography and correlated elemental analysis of hybrid perovskite microstructures: An insight into defect-related lattice distortion and photoinduced ion migration. *J. Phys. Chem. Lett.* **2016**, *7*, 5227−5234.
(27) Li, Y.; Galisteo-Lopez, J. F.; Calvo, M. E.; Miguez, H. Facile synthesis of hybrid organic-inorganic perovskite microcubes of optical quality using polar antisolvents. *ACS Appl. Mater. Interfaces* **2017**, *9*, 35505−35510.
(28) Zhang, F.; Zhong, H.; Chen, C.; Wu, X.-g.; Hu, X.; Huang, H.; Han, J.; Zou, B.; Dong, Y. Brightly luminescent and color-tunable colloidal $CH_3NH_3PbX_3$ (X = Br, I, Cl) quantum dots: Potential alternatives for display technology. *ACS Nano* **2015**, *9*, 4533−4542.
(29) Ning, Z.; et al. Quantum-dot-in-perovskite solids. *Nature* **2015**, *523*, 324−328.
(30) Baghbanzadeh, M.; Belding, L.; Yuan, L.; Park, J.; A-Sayah, M. H.; Bowers, C. M.; Whitesides, G. M. Dipole-induced rectification across Ag^{TS}/SAM//Ga_2O_3/EGaln junctions. *J. Am. Chem. Soc.* **2019**, *141*, 8969−8980.
(31) Shi, D.; et al. Low trap-state density and long carrier diffusion in organolead trihalide perovskite single crystals. *Science* **2015**, *347*, 519−522.
(32) Pandey, K.; Chauhan, M.; Bhatt, V.; Tripathi, B.; Yadav, P.; Kumar, M. High-performance self-powered perovskite photodetector with a rapid photoconductive response. *RSC Adv.* **2016**, *6*, 105076−105080.
(33) Liu, Y.; et al. Two-inch-sized perovskite $CH_3NH_3PbX_3$ (X = Cl, Br, I) crystals: Growth and characterization. *Adv. Mater.* **2015**, *27*, 5176−5183.
(34) Ma, H.; et al. Interface state-induced negative differential resistance observed in hybrid perovskite resistive switching memory. *ACS Appl. Mater. Interfaces* **2018**, *10*, 21755−21763.
(35) Xiao, Z.; Yuan, Y.; Shao, Y.; Wang, Q.; Dong, Q.; Bi, C.; Sharma, P.; Gruverman, A.; Huang, J. Giant switchable photovoltaic effect in organometal trihalide perovskite devices. *Nat. Mater.* **2015**, *14*, 193−198.
(36) Li, C.; Tscheuschner, S.; Paulus, F.; Hopkinson, P. E.; Kiessling, J.; Koehler, A.; Vaynzof, Y.; Huettner, S. Iodine migration and its effect on hysteresis in perovskite solar cells. *Adv. Mater.* **2016**, *28*, 2446−2454.
(37) Liu, J.; Yin, X.; Liu, X.; Que, M.; Que, W. Multi-influences of ionic migration on illumination-dependent electrical performances of inverted perovskite solar cells. *J. Phys. Chem. C* **2017**, *121*, 16051−16057.
(38) Deng, Y.; Xiao, Z.; Huang, J. Light-induced self-poling effect on organometal trihalide perovskite solar cells for increased device efficiency and stability. *Adv. Energy Mater.* **2015**, *5*, 1500721.
(39) Yoo, E. J.; Lyu, M.; Yun, J.-H.; Kang, C. J.; Choi, Y. J.; Wang, L. Resistive switching behavior in organic-inorganic hybrid $CH_3NH_3PbI_{3-x}Cl_x$ perovskite for resistive random access memory devices. *Adv. Mater.* **2015**, *27*, 6170−6175.
(40) He, J.; Zhu, J.; Ma, C.; Lu, J.; Hu, Z. Negative differential resistance and multilevel resistive switching in $BaSrTiO_3$ films. *Appl. Phys. Lett.* **2019**, *115*, 072101.
(41) Gu, C.; Lee, J.-S. Flexible Hybrid Organic-Inorganic Perovskite Memory. *ACS Nano* **2016**, *10*, 5413−5418.
(42) Ding, J.; Fang, H.; Lian, Z.; Li, J.; Lv, Q.; Wang, L.; Sun, J.-L.; Yan, Q. A self-powered photodetector based on a $CH_3NH_3PbI_3$ single crystal with asymmetric electrodes. *CrystEngComm* **2016**, *18*, 4405−4411.
(43) Li, H.; Tao, L.; Huang, F.; Sun, Q.; Zhao, X.; Han, J.; Shen, Y.; Wang, M. Enhancing efficiency of perovskite solar cells via surface passivation with graphene oxide interlayer. *ACS Appl. Mater. Interfaces* **2017**, *9*, 38967−38976.
(44) Andricevic, P.; Mettan, X.; Kollar, M.; Nafradi, B.; Sienkiewicz, A.; Garma, T.; Rossi, L.; Forro, L.; Horvath, E. Light-emitting electrochemical cells of single crystal hybrid halide perovskite with vertically aligned carbon nanotubes contacts. *ACS Photonics* **2019**, *6*, 967−975.
(45) Li, M.; et al. Ultrathin nanosheets of oxo-functionalized graphene inhibit the ion migration in perovskite solar cells. *Adv. Energy Mater.* **2020**, *10*, 1902653.

https://dx.doi.org/10.1021/acs.nanolett.0c03347
Nano Lett. 2020, 20, 8640−8646